This is an *Accepted Manuscript*, which has been through the Royal Society of Chemistry peer review process and has been accepted for publication.

Accepted Manuscripts are published online shortly after acceptance, before technical editing, formatting and proof reading. Using this free service, authors can make their results available to the community, in citable form, before we publish the edited article. We will replace this *Accepted Manuscript* with the edited and formatted *Advance Article* as soon as it is available.

You can find more information about *Accepted Manuscripts* in the **Information for Authors**.

Syntheses, structures, and properties of six cobalt(II) complexes

based on a tripodal tris(4-(1*H*-1,2,4-triazol-1-yl)phenyl)amine ligand

Zhenzhen Shi,[a] Zhaorui Pan,[a,b] Chuanlei Zhang,[a] Hegen Zheng[*,a]

Abstract: Six new cobalt(II) metal-organic frameworks, $\{[Co_{1.5}(TTPA)(BTC)(H_2O)]_2 \cdot 13H_2O\}_n$ (**1**), $[Co(TTPA)(PA)]_n$ (**2**), $\{[Co(TTPA)(BDA)_{0.5}(NO_3)] \cdot 3H_2O\}_n$ (**3**), $\{[Co_2(TTPA)_3(OBA)_2(H_2O)_3] \cdot 2CH_3CN \cdot 4H_2O\}_n$ (**4**), $\{[Co(TTPA)(AIP)(H_2O)] \cdot 2H_2O\}_n$ (**5**), and $\{[Co(TTPA)(MIP)(H_2O)] \cdot 2H_2O\}_n$ (**6**), have been prepared from the self-assembly of tris(4-(1H-1,2,4-triazol-1-yl)phenyl)amine (TTPA) ligand with different aromatic carboxylate auxiliary ligands (H_3BTC = 1,3,5-benzenetricarboxylic acid, H_2PA = phthalic acid, H_2BDA = (1,1'-biphenyl)-4,4'-dicarboxylic acid, H_2OBA = 4,4'-oxydibenzoic acid, H_2AIP = 5-aminoisophthalic acid, H_2MIP = 5-methylisophthalic acid) and cobalt salts. Their structures have been characterized by infrared spectroscopy, elemental analysis, single crystal X-ray analysis, powder X-ray diffraction. Complex **1** is an unusual 4-nodal (3,3,4,8)-connected three-dimensional (3D) new topological net with point symbol of $(4.6.8)_4(4^4.6^7.8^{15}.10^2)(6^2.8^4)$. Complex **2** has a 2-fold interpenetrating 3D **dia** framework. Complex **3** displays a rare binodal (3,4)-connected 4-fold interpenetrating 3D architecture with a **fsc**-3,4-*C2/c* topology with point symbol of $(4.6.8)(4.6^2.8^3)$. Complex **4** shows two distinct two-dimensional (2D) layers with **hcb** topologies, which are further packed into a 3D structure by O-H⋯O hydrogen bonding interactions. Both complexes **5** and **6** feature similar 2D sheets with **sql** topologies, which can be further packed into a 3D structure by O-H⋯O hydrogen bonding interactions. Moreover, the thermal stability and UV-visible spectra of these complexes are also discussed in detail. Meanwhile, variable-temperature magnetic susceptibility measurement of complex **1** reveals

antiferromagnetic interactions between Co(II) ions.

Introduction

The rational design and construction of metal-organic frameworks (MOFs) have been pursued for many years because of their intriguing topologies,[1-3] and potential applications in nonlinear optics,[4] molecular magnetism,[5] gas storage and separation,[6-9] luminescence,[10-13] and so forth. In principle, self-assembly process of MOFs is complicated, which still remains a major challenge in this field because their constructions are influenced by many factors, such as organic ligands,[14-16] metal ions,[17,18] metal-ligand ratio,[19,20] solvent species,[21,22] temperature,[23,24] pH value,[24,25] and so on. To our knowledge, the selection of suitable organic ligands is very important for constructing extended coordination frameworks. Among them, the tripodal triphenylamine-based multidentate ligands are prominent for constructing porous MOFs with aesthetic topological structures.[26-28] Triphenylamine unit processes prominent electron donating ability but also hole-transport properties to modify effectively the electrical conductivities of the materials.[29,30] Especially, the N-donor ligands based on triphenylamine derivatives, such as tri(4-(1H-imidazol-1-yl)phenyl)amine (TIPA) [31-37] and tri(4-pyridylphenyl)amine (TPPA),[38-40] have been widely used in the construction of various coordination polymers with potential properties. Recently, Zhang Jian and co-workers in Fujian Institute of Research reported two cationic MOFs with large nanotubular channels, $[Zn_2(TIPA)_2(OH)]\cdot3NO_3\cdot12H_2O$ (FIR-53) and $[Zn(TIPA)]\cdot2NO_3\cdot DMF\cdot4H_2O$ (FIR-54) show fast ion exchange and high uptake capacity for $Cr_2O_7^{2-}$ through interesting single-crystal-to-single-crystal transformations.[28] Particularly, they noted FIR-53 shows the ability of the high and fast ion exchange as well as excellent reversibility. Considering the above mentioned, we introduce 1,2,4-triazole to the triphenylamine system and prepare new TTPA ligand having the integration of flexible and long rigid characters (Scheme 1, top). The TTPA ligand contains C-N bonds to make phenyl and triazole rings rotate freely and to more easily meet the

geometric and conformational requirement when coordinating to the metal ions. On the other hand, compared triazole rings with imidazole and pyridine rings of these ligands, TTPA ligand has more coordination sites. Moreover, MOFs based on the TTPA ligand are rarely known to date.
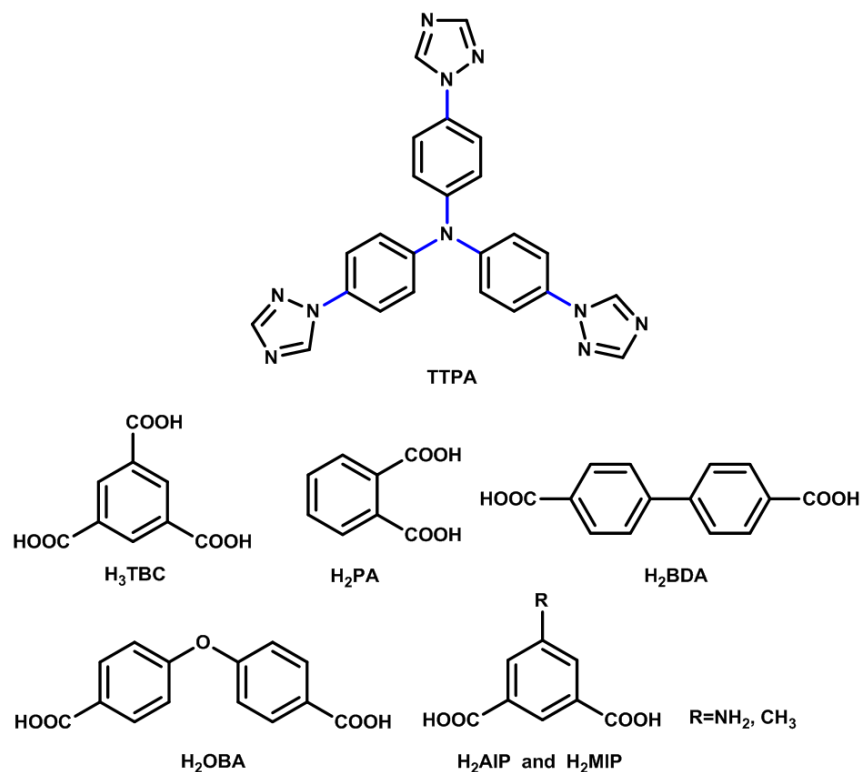
Scheme 1. TTPA and aromatic carboxylate ligands

Aromatic carboxylates are often employed as bridging ligands to construct MOFs because of their versatile coordination conformations, i.e., *syn-syn*, *syn-anti*, and *anti-anti*, etc.[3,41] These carboxylates bridged high-spin cobal(II) ions exhibit versatile coupling to mediate magnetic interactions and accomplish the transmission of magnetic coupling to different degrees.[42] In this full paper, we introduce TTPA ligand with different aromatic carboxylates as auxiliary ligands (Scheme **1**) and cobalt salts, and synthesize six new metal-organic frameworks, $\{[Co_{1.5}(TTPA)(BTC)(H_2O)]_2 \cdot 13H_2O\}_n$ (**1**), $[Co(TTPA)(PA)]_n$ (**2**), $\{[Co(TTPA)(BDA)_{0.5}(NO_3)] \cdot 3H_2O\}_n$ (**3**),

$\{[Co_2(TTPA)_3(OBA)_2(H_2O)_3]\cdot 2CH_3CN\cdot 4H_2O\}_n$ **(4)**,
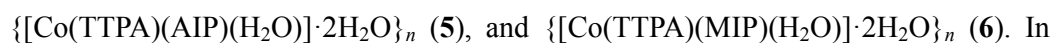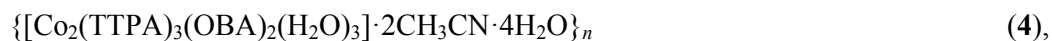
$\{[Co(TTPA)(AIP)(H_2O)]\cdot 2H_2O\}_n$ **(5)**, and $\{[Co(TTPA)(MIP)(H_2O)]\cdot 2H_2O\}_n$ **(6)**. In

addition, we also describe their characterizations and properties in detail.

Results and discussion

The experimental section has been listed in the Electronic Supplementary Information

(ESI). Crystallographic data and experimental details for complexes **1-6** are given in

Table 1. Selected bond lengths and angles of these complexes are listed in Table S1

(ESI), hydrogen bonding distance and angle data for complexes **1** and **3-6** are listed in

Table S2.

Description of crystal structures

$\{[Co_{1.5}(TTPA)(BTC)(H_2O)]_2\cdot 13H_2O\}_n$ (1)

Single crystal X-ray structural analysis reveals that complex **1** crystallizes in the

triclinic crystal system, space group $P\bar{1}$. The asymmetric unit consists of one and a

half Co(II) ions, one deprotonated H_3BTC ligand, one TTPA ligand, one coordinated

water molecule and six and a half lattice water molecules (four and a half of these

lattice water molecules were squeezed by PLATON[43]). As shown in Fig 1a, there are

two crystallographic independent Co(II) ions in **1**, both of which are six-coordinated

with slightly distorted $\{CoN_2O_4\}$ octahedral coordination geometries. Co1 ion is

coordinated by four carboxylate oxygen atoms from three different BTC^{3-} ligands at

the equatorial positions and two nitrogen atoms from two TTPA ligands at the axial

positions with the N(1)-Co(1)-N(8)#3 angles of 179.63(10) °. While Co2 ion is

coordinated by two carboxylate oxygen atoms from two different BTC^{3-} ligands and

two nitrogen atoms from TTPA ligands at the equatorial positions as well as two

oxygen atoms from two coordinated water molecules at the axial positions with the

O(7)W-Co(2)-O(7)W#4 angles of 179.998(1) °. The Co-O bond lengths are in the

range of 2.0235(19)−2.224(2) Å, and the Co-N ones are in the range of

2.120(3)−2.131(3) Å, respectively.

TTPA ligands adopting μ_3-bridge coordination modes (Fig S1a, ESI) link Co1 and Co2 ions to generate a 1D ladder-like chain along the *bc* plane (Fig 1b). Such adjacent chains are further connected by BTC[3-] ligands, leading to the formation of a porous 3D framework (Fig 1c). Better insight into the complicated 3D frameworks, it is noted that two deprotonated carboxylic groups of H$_3$BTC ligands adopting μ_2-η^1:η^1 and μ_1-η^1:η^1 coordination modes (Fig S2a), link Co1 ions to form an infinite 1D chain composed of binuclear Co$_2$(CO$_2$)$_4$ second building units (SBUs). The third deprotonated carboxylic group of H$_3$BTC ligands adopting μ_1-η^0:η^1 coordination mode (Fig S2a) between these infinite 1D chains, link Co2 ions to generate the 2D layer composed of binuclear Co$_2$(CO$_2$)$_4$ SBUs and mononuclear Co2 nodes along the *ab* plane (Fig 1d). The distances between two Co1 ions in the SBUs containing 8-membered rings are 4.44 Å. The adjacent SBUs are bridged through BTC[3-] ligands to form a 1D chain, at the same time generating 16-membered rings in which the nearest distance between two Co1 ions are 6.98 Å. As shown in Fig 1d, the 2D layer is further connected by O-H···O hydrogen bonding interactions. Lattice water molecules (O8W and O9W) located in the channel of the layer are fixed by multiform hydrogen bonding, and bonded to coordinated water molecules (O7W) and carboxylate oxygen atoms (O1 and O3) of the host framework (Fig S3a). These hydrogen-bonding interactions bring further stability for these 2D layer structures. The hydrogen-bonding metrics and bond parameters are also shown in Table S2. There also exist channels (Fig 1e) with a cross-section of approximately 16.2 × 10.2 Å (excluding van der Waals radii) in the 3D framework. Complex **1** contains solvents accessible void space of 51% (1453.7 Å^3 per unit cell) of the total crystal volume as calculated by PLATON program.

To better understand the nature of this intricate structure, a TOPOS analysis is provided by software TOPOS 4.0.[44] Both TTPA and BTC[3-] ligands can be regarded as 3-connected nodes, while Co$_2$(CO$_2$)$_4$ SBUs and Co2 ions act as 8-connected and 4-connected nodes, respectively. Therefore, the whole structure can thus be represented as a new 4-nodal 3,3,4,8-connected net (Fig 1f) with point symbol of $(4.6.8)_4(4^4.6^7.8^{15}.10^2)(6^2.8^4)$.
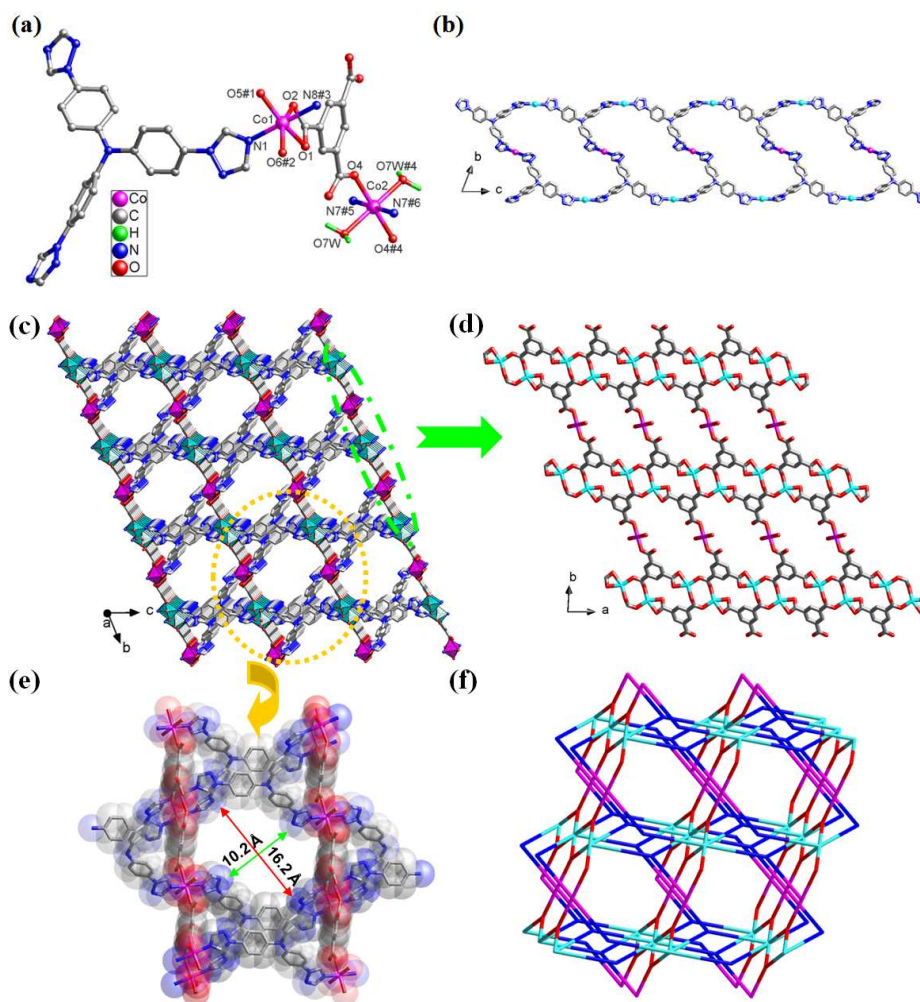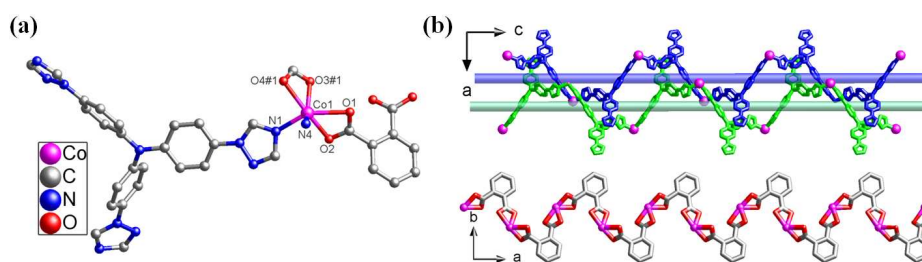
Fig 1. (a) Coordination environment of Co(II) ions in **1**. The lattice water molecules and hydrogen atoms are omitted for clarity. Symmetry codes: #1 = $-x + 2, -y + 1, -z + 1$; #2 = $x - 1, y, z$; #3 = $x, y, z + 1$; #4 = $-x + 3, -y, -z + 1$; #5 = $-x + 3, -y + 1, -z$; #6 = $x, y - 1, z + 1$. (b) A 1D ladder-like chain constructed by Co(II) ions and TTPA ligands of **1**. (c) The 3D porous framework of **1**. (d) A 2D layer is linked by Co(II) ions and BTC^{3-} ligands of **1**. (e) The channel in **1** along the a axis. (f) Schematic view of 3,3,4,8-connected topology of **1**. (Co$_2$(CO$_2$)$_4$ SBUs or Co1 ions are turquoise, Co2 ions are pink, BTC^{3-} ligands are red, and TTPA ligands are blue)

[Co(TTPA)(PA)]$_n$ (2)

Crystal structure analysis of complex **2** was solved in the orthorhombic crystal system of *Pbca*. The structure of **2** contains a Co(II) ion, a TTPA ligand, and a deprotonated

H_2PA ligand. Each Co ion is six-coordinated by two nitrogen atoms from two different TTPA ligands and four oxygen atoms from two different PA^{2-} ligands to form a distorted $\{CoN_2O_4\}$ octahedral geometry (Fig 2a). The Co-N bond distances are 2.089(3) and 2.091(3) Å, respectively. And the Co-O bond distances are in the range of 2.035(3)−2.332(2) Å.

TTPA ligands adopting μ_2-bridge coordination modes (Fig S1b) link Co ions to generate 1D alternate left- and right-helical chains with a pitch of 25.86 Å along the c axis (Fig 2b, top). These 1D helical chains are further connected by PA^{2-} ligands, leading to the formation of a single 3D porous framework (Fig 2c). Better insight into the present 3D frameworks, it is clearly observed that all deprotonated carboxylic groups of H_2PA ligands adopt μ_1-η^1:η^1 coordination modes (Fig S2b), and link Co ions to form a 1D chain along the a axis (Fig 2b, bottom). From a topological perspective, the single 3D structure can be described as a 4-connected **dia** topology (Fig 2d). In order to minimize the presence of cavities (Fig 2e) with a cross-section of approximately 14.2 × 12.0 Å (excluding van der Waals radii) and to stabilize the structure during the assembly process, the other identical networks are filled in the voids yielding a 3D 2-fold interpenetrating network, as shown in the Fig 2f. The interpenetration can be classified as type *Class IIa*, Z = 2 ($Z_t = 1$; $Z_n = 2$).
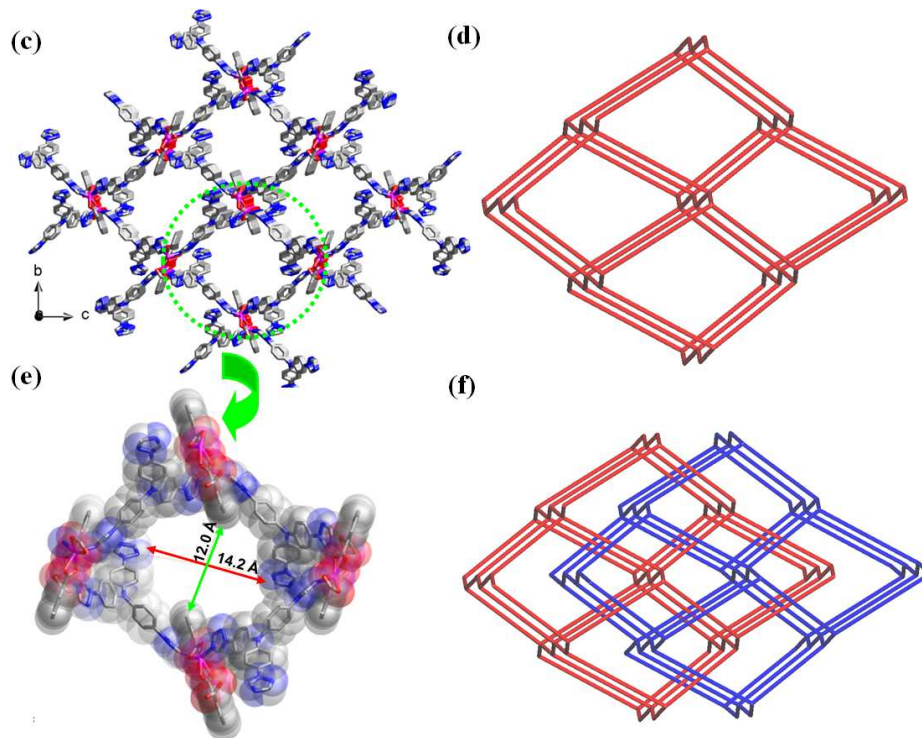
Fig 2. (a) Coordination environment of the Co(II) ions in **2**. The hydrogen atoms are omitted for clarity. Symmetry codes: #1 = $x - 1/2, -y + 3/2, -z + 2$. (b) The 1D chains constructed by Co(II) ions and TTPA or PA^{2-} ligands of **2** along the different direction respectively. (c) A single porous 3D framework of **2**. (d) The 4-connected **dia** topology of **2**. (e) The channel in a single porous framework of **2** along the *a* axis. (f) Schematic view of 2-fold interpenetration of **2**.

{[Co(TTPA)(BDA)$_{0.5}$(NO$_3$)]·3H$_2$O}$_n$ (3)

The crystal structure determination of complex **3** reveals that it crystallizes in the monoclinic crystal system, space group *C*2/*c*. The asymmetric unit contains a Co(II) ion, a TTPA ligand, half a deprotonated H$_2$BDA ligand, a nitrate ion and three lattice water molecules (one of these lattice water molecules was removed using PLATON). Each Co ion takes a slightly distorted {CoN$_3$O$_3$} octahedral coordination geometry, in which a nitrogen atom from a TTPA ligand and two carboxylate oxygen atoms from a BDA^{2-} ligand and an oxygen atom from a nitrate ion form the equatorial plane and the apical positions are occupied by two other nitrogen atoms from two different TTPA ligands with the N(1)-Co(1)-N(7)#2 angle of 173.07(10) °. The Co-N bond lengths

are in the range of 2.109(2)−2.126(3) Å, and the Co-O ones are 2.140(2)−2.228(2) Å, respectively.

TTPA ligands adopting μ_3-bridge coordination modes (Fig S1c) connect Co(II) ions to yield a 2D layer along the *ab* plane (Fig 3b). Such adjacent layers are further bridged by deprotonated carboxylic groups of H$_2$BDA ligands adopting μ_1-η^1:η^1 coordination modes (Fig S2c), giving rise to the formation of a 3D framework (Fig 3c). There exist channels with a cross-section of approximately 11.5 × 13.8 Å (excluding van der Waals radii) in the 3D framework (Fig 3d). There exist hydrogen-bonding interactions between carboxylate oxygen atoms (O1 and O2) and lattice water molecule (O1W), which bring further stability for these 3D frameworks. The hydrogen-bonding metrics and bond parameters are also shown in Table S2.

From a topological perspective, TTPA ligands and Co(II) ions act as 3-connected and 4-connected nodes, while BDA ligands can be treated as linkers. Thus, **3** can be interpreted as a (3,4)-connected **fsc**-3,4-*C2/c* net with the point symbol of $(4.6.8)(4.6^2.8^3)$ (Fig 3e). It is noticed that only two examples of (3,4)-connected **fsc**-3,4-*C2/c* net have been reported by Chen et al.[45] and our group.[46] The potential voids are large enough to be filled via mutual interpenetration of four independent 3D frameworks, generating a 4-fold interpenetrating 3D structure (Fig 3f). The interpenetration can be classified as type *Class Ib*, Z = 4 (Z_t = 2*2; Z_n = 1) (the interpenetrated nets are generated by more translations and partial interpenetration vectors (PIVs) are [0,1,0] (12.54 Å), [1/2,1/2,0] (15.64 Å), and [1/2,-1/2,0] (15.64 Å)). Despite 4-fold interpenetration of complex **3**, there still exists the potential void space of 27.2% (2058.3 Å^3 per unit cell) of the total crystal volume calculated by PLATON after removal of guest water molecules.
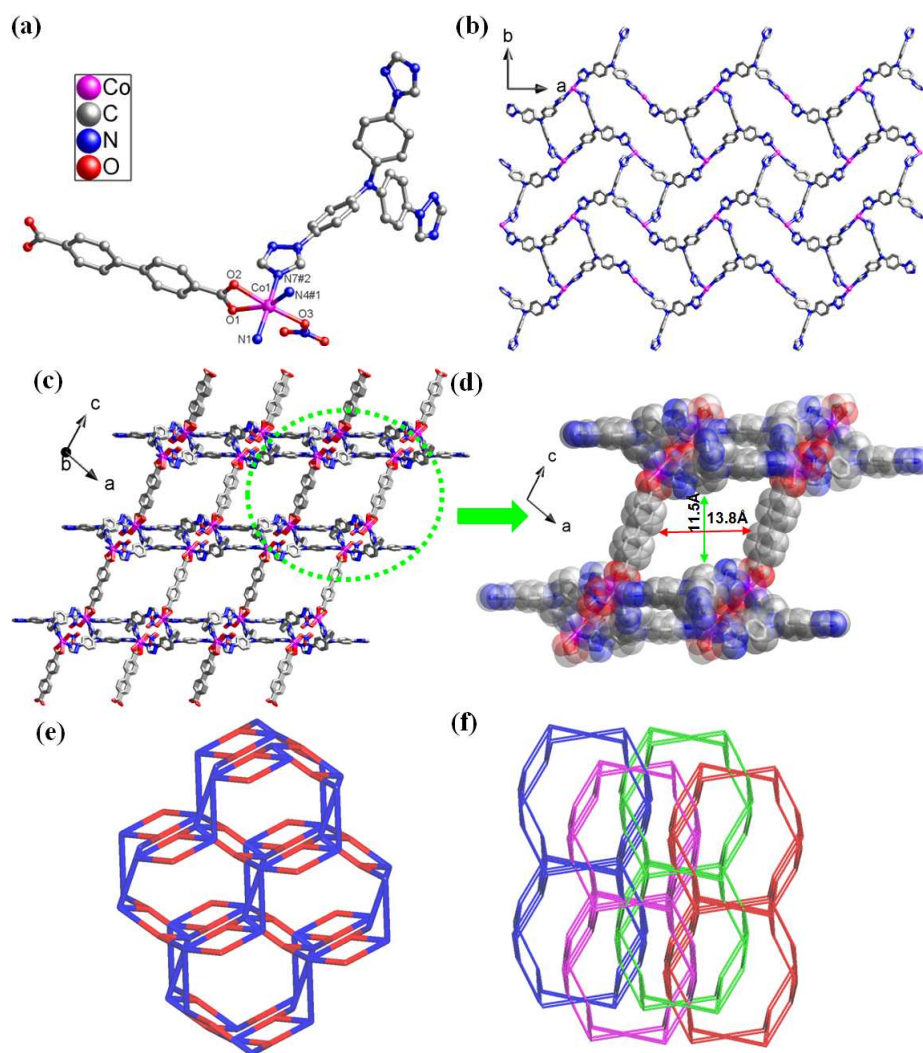
Fig 3. (a) Coordination environment of the Co(II) ions in **3**. The lattice water molecules and hydrogen atoms are omitted for clarity. Symmetry codes: #1 = $- x, y + 1, - z + 1/2$; #2 = $x + 1/2, - y + 3/2, z + 1/2$. (b) A 2D layer constructed by Co(II) ions and TTPA ligands of **3**. (c) A single 3D framework of **3**. (d) View of the channel in **3**. (e) A single 3D framework with a **fsc**-3,4-*C2/c* topology of **3** (Co(II) ions are blue and TTPA ligands are red). (f) 4-fold interpenetrating framework of **3**.

[Co₂(TTPA)₃(OBA)₂(H₂O)₃]·2CH₃CN·4H₂O}ₙ (4)

Single-crystal X-ray characterization indicates that complex **4** comprises two crystallographically distinct 2D polymeric motifs, that is, two puckered Shubnikov hexagonal plane nets (**hcb**) of [Co(TTPA)(OBA)(H₂O)₂] and [Co(TTPA)₂(OBA)(H₂O)]. It crystallizes in the triclinic crystal system, space group

*P*1. The asymmetric unit contains two crystallographic independent Co(II) ions, three TTPA ligands, two deprotonated H₂OBA ligands, three coordinated water molecules, two CH₃CN solvent molecules and four lattice water molecules (three of these lattice water molecules were squeezed by PLATON). As shown in Fig 4a, both of crystallographic independent Co(II) atoms are six-coordinated with a distorted octahedral environment ($\{CoN_3O_3\}$ for Co1; $\{CoN_4O_2\}$ for Co2). Co1 ion is coordinated by three nitrogen atoms from three different TTPA ligands and an oxygen atom from a coordinated water molecule at the equatorial positions and two other oxygen atoms from a OBA²⁻ ligand and a coordinated water molecule at the axial positions with the O2W-Co1-O1 angles of 176.97(17) °. Different from the Co1, one coordinated site is occupied at the equatorial position by one nitrogen atom from one TTPA ligand in Co2 instead of one oxygen atom from one coordinated water molecule. The apical positions are occupied by two oxygen atoms with the O3W-Co2-O6 angles of 173.79(16) °. The Co-N distances are 2.122(5) to 2.198(4) Å, and the Co-O distances range from 2.039(3) to 2.097(3) Å, respectively.

TTPA ligands adopting μ_3-bridged coordination modes (Fig S1d) link three Co1 ions to form a 2D layer labeled A (Fig 4b). But Co2 ions are linked by TTPA ligands adopting μ_3- or μ_1-bridged coordination modes (Fig S1e and 1f) to form the other 2D layer labeled B (Fig 4c). Both layer A and layer B are packed in an orderly ABAB-type array by O-H···O hydrogen bonding interactions (Table S2) to form a 3D structures (Fig S3b). One carboxylate group of the H₂OBA ligand adopting μ_1-η^1:η^0 coordination mode is deprotonated (Fig S2d). However, the other deprotonated carboxylate group of the H₂OBA ligand doesn't take part in coordinating with Co(II) ion but balances charge in the frameworks. To analyze the topology of complex **4**, both TTPA ligands and Co(II) centers could be simplified as 3-connected nodes. Two simplified layers are shown in Fig 4d. These layers belong to 3-connected 6³-**hcb** topologies.

(a)

(b)

A

(c)

B

(d)
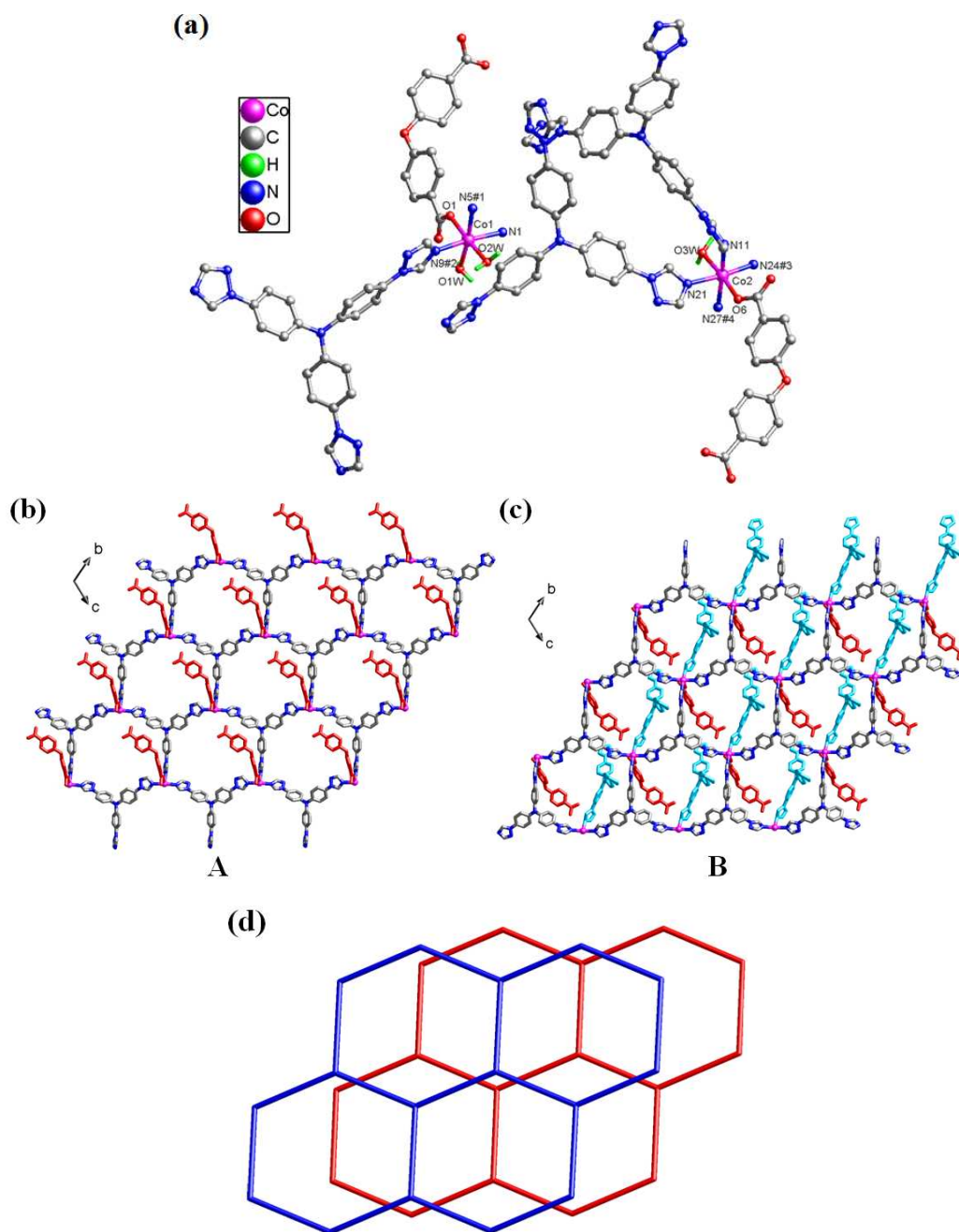

Fig 4. (a) Coordination environment of the Co(II) ions in two motifs in **4**. The CH_3CN, lattice water molecules and hydrogen atoms are omitted for clarity. Symmetry codes: #1 = x, y + 1, z; #2 = x, y + 1, z + 1; #3 = x, y − 1, z − 1; #4 = x, y − 1, z. (b) and (c) Two different 2D polymeric layer A and B of **4**. (d) Schematic view of **hcb** topologies of layer A and B of **4**.

{[Co(TTPA)(AIP)(H$_2$O)]·2H$_2$O}$_n$ (5) and {[Co(TTPA)(MIP)(H$_2$O)]·2H$_2$O}$_n$ (6)

Complexes **5** and **6** crystallize in the same triclinic crystal system of space group

$P\bar{1}$and have similar cell parameters. The results of crystal structure analyses reveal

that they indeed have the similar structures. Thus, only the structure of **5** is described

here. The crystal structure of **5** exhibits a 2D layer with **sql** topology. The asymmetric

unit consists of one Co(II) ion, one TTPA ligand, one deprotonated H$_2$AIP ligand, one

coordinated water molecule and two lattice water molecules (one of these lattice water

molecules was removed using PLATON). As shown in Fig 5a, Co1 shows a slightly

distorted {CoN$_2$O$_4$} octahedral coordination geometry, which is six-coordinated by

three carboxylate oxygen atoms from two AIP^{2-} ligands and an oxygen atom from a

coordinated water molecule at the equatorial positions and two nitrogen atoms from

two TTPA ligands at the axial positions with the N4#2-Co1-N1 angles of 177.82(10) °.

The Co-O bond lengths are in the range of 2.050(2)–2.289(2) Å, and the Co-N ones

are 2.128(3) and 2.143(2) Å, respectively. TTPA ligands adopting μ_2-bridged

coordination modes (Fig S1g) link Co ions to form 1D chains. Then the deprotonated

carboxylic groups of H$_2$AIP ligand adopt μ_1-η^1:η^1 and μ_1-η^0:η^1 coordination modes

(Fig S2e), and connect these adjacent 1D chains to form 2D layer (Fig 5b). Adjacent

2D layers are packed in an orderly ABAB-type array (Fig 5c) by O-H···O hydrogen

bonding interactions between coordinated oxygen atoms and solvent water molecules

(Table S2) along the c axis. Analysis of the network topology of **5** reveals that each

Co(II) ion plays a 4-connected node. Two simplified layers are shown in Fig 5d. Thus,

they can be represented as 4-connected **sql** topologies with point symbol of $(4^2.6^2)$
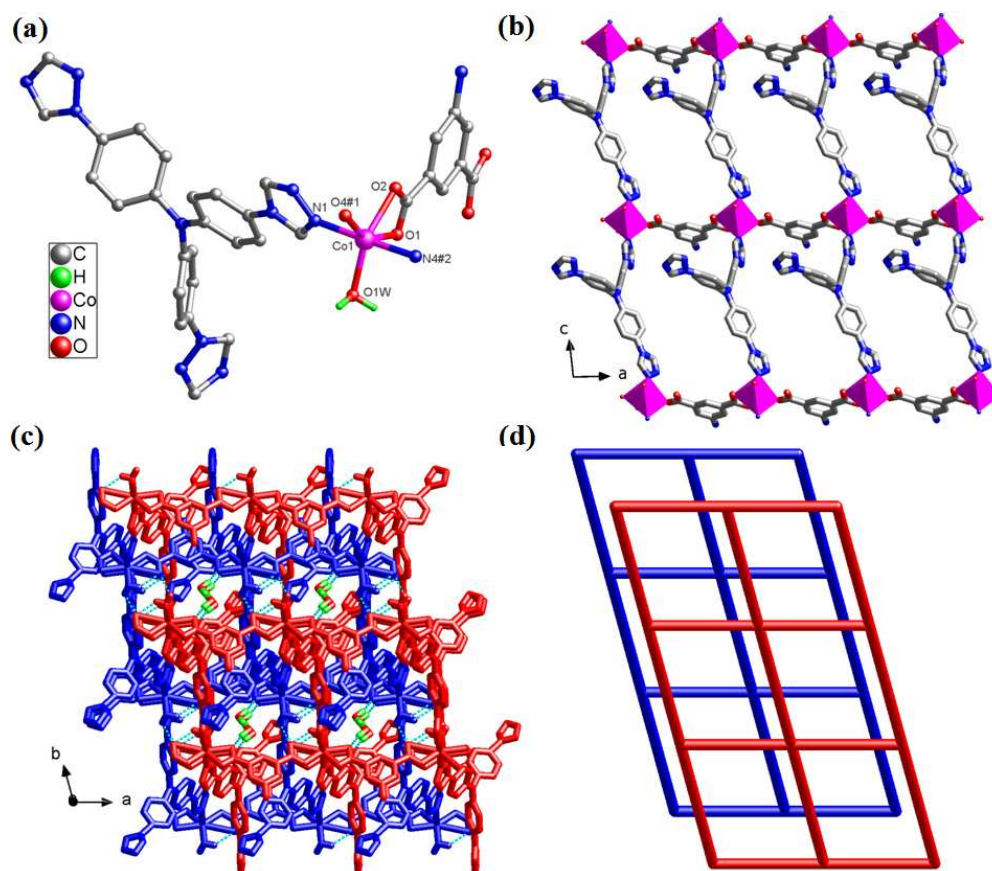
(Fig 5d).

Fig 5. (a) Coordination environment of the Co(II) ions in **5**. The lattice water molecules and hydrogen atoms are omitted for clarity. Symmetry codes: #1 = *x* + 1, *y*, *z*; #2 = *x*, *y* − 1, *z* − 1. (b) A single 2D layer of **5**. (c) Perspective view of the ···ABAB··· stacking 3D structure by hydrogen bonding interactions (turquoise dashed lines) of **5**. (d) Schematic view of **sql** topologies of **5**.

Effect of the organic ligands on networks

From the above discussion, it can be seen that TTPA ligand and the anionic carboxylate-involved ligands play a critical role in assembling the resulting networks with diverse topologies. In these complexes, coordinated nitrogen atoms of triazole rings in the TTPA ligand display different degrees and bridging fashions (Fig S1: a for **1**, b for **2**, c for **3**, d-f for **4**, g for **5** and h for **6**). As for **1-6**, the aromatic tricarboxyl or dicarboxyl co-ligands are fully deprotonated and show various connection modes with the Co(II) centers (Fig S2). A comparison of the crystal

structures of **1** and **2** clearly indicates that the auxiliary O-donor ligands have a significant influence on structural assembly of coordination architectures. When the 3-connected BTC[3-] ligand is introduced, a porous 3D framework of **1** with a new 3,3,4,8-connected 4-nodal topology is obtained. However, 2-connected PA[2-] ligand is adopted, complex **2** displays 3D coordination frameworks with 2-fold interpenetrating **dia** topology. When changing the PA[2-] ligand to the longer BDA[2-] ligand, a 4-fold interpenetrated **fsc**-3,4-*C2/c* architecture of **3** is obtained. Although TTPA adopt μ_3- or μ_1-bridge coordination modes in **4**, V-shaped OBA[2-] ligand shows terminal mode. As a result, **4** shows two 2D layers, respectively. The connectivity of organic ligands in complexes **5** and **6** is same, so they have similar structures. These 2D layers of **4-6** are held together by O-H···O hydrogen bonding interactions between solvent waters and oxygen atoms of carboxylate to generated 3D supramolecular structures.

Powder X-ray diffraction and thermogravimetric analyses

In order to confirm the purities of complexes **1-6**, the powder X-ray diffraction (PXRD) analyses of these complexes were carried out at room temperature. As shown in Fig S4-S9, the main peak positions of the experimental patterns of **1-6** are almost consistent with their simulated ones, demonstrating single phase purities of the products.

To examine the thermal stabilities of complexes **1-6**, TG analyses were carried out (Fig 6). The TG study of complex **1** shows a weight loss of 15.23% (calc. 15.40%) from 25 to 158 °C, suggesting that the all solvent waters molecules and two coordinated water molecules are removed. Above 400 °C, a rapid weight loss is observed, which is attributed to the decomposition of coordination framework. There is almost no weight loss for complex **2** from room temperature to 340 °C, which indicates that it has relatively higher thermal stability. Then its framework begins to collapse. For complex **3**, a weight loss of 7.88% (calc. 7.29%) is observed from 25 to 200 °C which is attributed to the loss of the three lattice water. Then one coordinated nitrate anion is gradually lost in the range of 200–285 °C (calc. 8.36%, exp. 8.83%).

Finally, the decomposition of the structure begins. The TG curve of complex **4** indicates that there is an initial weight loss of approximately 6.87% between room temperature and 140 °C, corresponding to the loss of guest molecules (6.82% calc. for two CH$_3$CN and four lattice water molecules per unit formula). After three coordinated water molecules are removed about 220 °C, corresponding to a little mass loss of about 2.48% (calc. 2.30%), then TG curve of **4** presents a gravity platform and the framework starts to decompose at 305 °C. Both complex **5** and **6** lose two lattice water molecules and one coordinated water molecule below 250 °C (calc. 7.33%, exp. 7.18% for **5**; calc. 7.33%, exp. 7.18% for **6**), then TG curves present a platform until approximately 370 °C and their frameworks start to decompose.
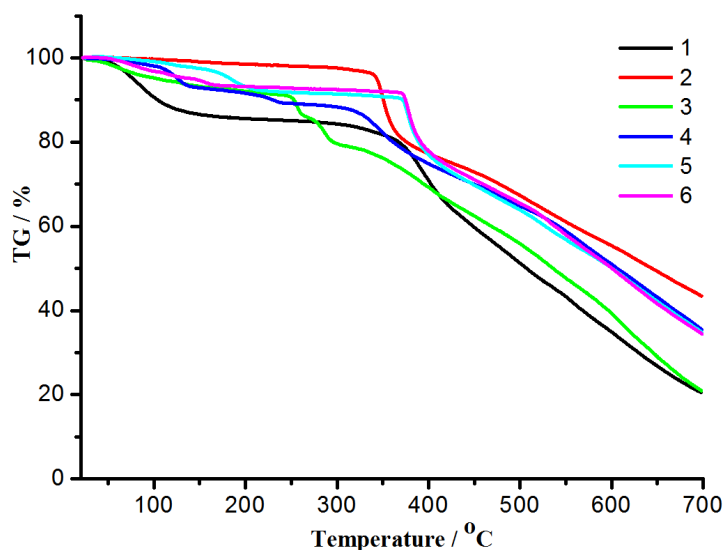

Fig 6. The TG diagrams of complexes **1-6**.

Photochemical properties

The solid-state UV-vis absorption spectra of TTPA ligand, auxiliary ligands and complexes **1–6** were carried out at room temperature. The absorption peaks at 290 nm (H$_3$BTC), 248 and 295 nm (H$_2$PA), 319 nm (H$_2$BDA), 280 nm (H$_2$OBA), 301 nm (H$_2$AIP), and 310 nm (H$_2$MIP) are shown in the Fig S10a, which can be ascribed to $\pi \rightarrow \pi^*$ or $n \rightarrow \pi^*$ transitions of these ligands, respectively. The TTPA ligand displays distinct absorption band in the UV range of 200–415 nm. We observe that complexes

1-6 have the similar higher energy bands in the range of 200–415 nm, which are considered as intraligand charge transfer transitions. Moreover, we observe the absorption peaks (Fig S10b) at 520 nm for **1**, 564 nm for **2**, 525 nm for **3**, 492 nm for **4**, 516 nm for **5**, and 513 nm for **6**, respectively, which can be assigned to the $^4T_{1g}(F)$ → $^4T_{1g}(P)$ transitions. Besides, there are additional shoulder peaks at 702 nm for **1**, 705 nm for **3**, 670 nm for **5**, and 660 nm for **6**, respectively, which may be ascribed to $^4T_{1g}(F)$ → $^4A_{2g}(F)$ transitions. In the visible region, these peaks are typical for octahdrally coordinated Co(II) complexes.[47-51] To explore the semiconductivity, the diffuse reflectance data is transformed into Kubelka−Munk function to obtain their band gaps (E_g). As shown in Fig S10c, the band gap of TTPA ligand is approximately 2.89 eV, which exhibit the nature of semiconductivity. The E_g values assessed from the steep absorption edges are 1.72 eV and 2.88 eV for **1**, 1.58 eV and 2.38 eV for **2**, 1.87 eV and 2.74 eV for **3**, 1.92 eV and 2.86 eV for **4**, 1.52 eV, 1.86 eV and 2.97 eV for **5**, 1.58 eV, 1.91 eV and 2.89 eV for **6**, respectively, which are estimated to be greater than the semiconductor silicon material with a band gap of 1.1 eV. So these complexes show optical band gaps which are characteristic for optical semiconductors.

Magnetic properties

The magnetic properties of crystalline samples **1** in the form of χ_M and $\chi_M T$ versus T plots (χ_M is the magnetic susceptibility per three Co(II) ions) in the temperature range 1.8−300 K under applied dc fields of 2000 Oe are shown in Fig 7. The $\chi_M T$ at room temperature is 6.7 cm^3 mol^{-1} K, which is higher than the spin-only value of 5.63 cm^3 mol^{-1} K expected for three isolated Co(II) ions (S = 3/2 with g = 2.0), indicating the contribution of spin-orbit coupling effects for the $^4T_{1g}$ ground term of high-spin Co(II) ion in octahedral field. Upon cooling, $\chi_M T$ gradually decreases and finally reach a value of 5.0 cm^3 mol^{-1} K at 1.8 K. The magnetic susceptibilities follow the Curie–Weiss law with C = 6.79 cm^3 mol^{-1} K and θ = −4.23 K, as shown in Fig S11. The above characteristics suggest antiferromagnetic interactions among Co(II) ions bridged carboxylic groups of BTC^{3-} ligands of **1**.
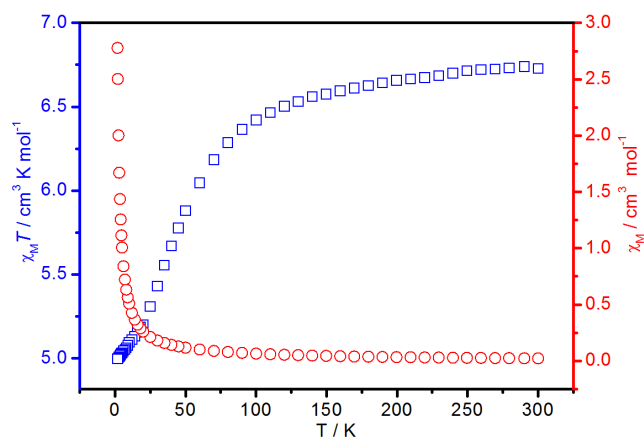
Fig 7. Temperature dependence of $\chi_M T$ and χ_M versus T for complex **1**.

Conclusions

In summary, we successfully synthesized six Co(II) complexes, which were constructed from TTPA ligand in the presence of different aromatic carboxylate ligands under hydrothermal conditions. Complex **1** is an unusual 4-nodal (3,3,4,8)-connected 3D new topological net with point symbol of $(4.6.8)_4(4^4.6^7.8^{15}.10^2)(6^2.8^4)$. Complex **2** has a 2-fold interpenetrating 3D **dia** framework with PA^{2-} ligand. When changing the PA^{2-} ligand to the longer BDA^{2-} ligand, a 4-fold interpenetrated **fsc**-3,4-*C2/c* architecture **3** is obtained. Complexes **4-6** are all 2D layers, while complex **4** shows two crystallographically distinct 2D polymeric layers with **hcb** topologies, which are further packed into a 3D supramolecular structures by O-H···O hydrogen bonding interactions. Both complex **5** and **6** feature similar 2D networks with **sql** topology, which can further packed into 3D frameworks by O-H···O hydrogen bonding interactions. The structural difference of these complexes may be attributed to the different bridging fashions of TTPA and auxiliary ligands. Optical absorption spectra of **1-6** indicate the nature of semiconductivity. Variable-temperature magnetic susceptibility measurements of complex **1** reveals antiferromagnetic interactions between Co(II) ions. The further exploitation of potential applications on MOFs with TTPA ligands will be underway.

Dalton Transactions Accepted Manuscript

Acknowledgment

Notes and references

[a]State Key Laboratory of Coordination Chemistry, School of Chemistry and Chemical Engineering, Collaborative Innovation Center of Advanced Microstructures, Nanjing University, Nanjing 210093, P. R. China.

[b]School of Environmental Science, Nanjing Xiaozhuang University, Nanjing 211171, P. R. China.

*E-mail: zhenghg@nju.edu.cn (H.G. Z.). Fax: 86-25-83314502.

Electronic Supplementary Information (ESI) available: Detailed experimental procedures, conformation of TTPA, coordination modes of auxiliary ligands, some additional figures, IR, PXRD and patterns of photochemistry; X-ray crystallographic data in CIF format and selected bond lengths and angles for **1-6**. CCDC: 1414118 -1414123. See DOI: 10.1039/x0xx00000x.

1. M. Eddaoudi, D. F. Sava, J. F. Eubank, K. Adila, V. Guillerma, *Chem. Soc. Rev.*, 2015, **44**, 228.

2. M. Li, D. Li, M. O'Keeffe, O. M. Yaghi, *Chem. Rev.*, 2014, **114**, 1343.

3. H. Furukawa, K. E. Cordova, M. O'Keeffe, O. M. Yaghi, *Science.*, 2013, **341**, 1230444.

4. L. L. Wen, L. Zhou, B. G. Zhang, X. G. Meng, H. Qu, D. F. Li, *J. Mater. Chem.*, 2012, **22**, 22603.

5. C. I. Yang, P. H. Chuang, G. H. Lee, S. M. Peng, K. L. Lu, *Inorg. Chem.*, 2012, **51**, 757.

6. Y. B. He, W. Zhou, G. D. Qian, B. L. Chen, *Chem. Soc. Rev.*, 2014, **43**, 5657.

7. E. D. Bloch, W. L. Queen, R. Krishna, J. M. Zadrozny, C. M. Brown, J. R. Long,

Science., 2012, **335**, 1606.

8. J. R. Li, J. L.Sculley, H. C. Zhou, *Chem. Rev.*, 2012, **112**, 869.

9. S. Q. Ma, D. F. Sun, X. S. Wang, H. C. Zhou, *Angew. Chem. Int. Ed.*, 2007, **46**, 2458.

10. S. S. Nagarkar, T. Saha, A. V. Desai, P. Talukdar, S. K. Ghosh. *Scientific Reports.*, 2014, **4**, 7053.

11. X. X. Li, H. Y. Xu, F. Z. Kong, R. H. Wang, *Angew. Chem. Int. Ed.*, 2013, **52**, 13769.

12. N. B. Shustova, A. F. Cozzolino, S. Reineke, M. Baldo, M. Dincă, *J. Am. Chem. Soc.*, 2013, **135**, 13326.

13. Y. J. Cui, Y. F. Yue, G. D. Qian, B. L. Chen, *Chem. Rev.*, 2012, **112**, 1126.

14. A. M. Plonka, D. Banerjee, J. B. Parise, *Cryst. Growth Des.*, 2012, **12**, 2460.

15. Q. Yang, X. F. Zhang, J. P. Zhao, B. W. Hu, X. H. Bu, *Cryst. Growth Des.*, 2011, **11***, 2839.

16. X. C. Huang, Y. Y. Lin, J. P. Zhang, X. M. Chen, *Angew. Chem. Int. Ed.*, 2006, **45**, 1557.

17. R. F. Jin, S. Y. Yang, H. M. Li, L. S. Long, R. B. Huang, L. S. Zheng, *CrystEngComm.*, 2012, **14**, 1301.

18. B. Y. Li, G. H. Li, D. Liu, Y. Peng,; X. J. Zhou, J. Hua, Z. Shi, S. H. Feng, *CrystEngComm.*, 2011, **13**, 1291.

19. F. H. Zhao, S. Jing, Y. X. Che, J. M. Zheng, *CrystEngComm.*, 2012, **14**, 4478.

20. X. P. Yang, R. A. Jones, M. M. Oye, M. Wiester, R. J. Lai, *New J. Chem.*, 2011, **35**, 310.

21. Q. X. Yang, X. Q. Chen, Z. J. Chen, Y. Hao, Y. Z. Li, Q. Y. Lu, H. G. Zheng, *Chem. Commun.*, 2012, **48**, 10016.

22. L. N. Li, S. Y. Wang, T. L. Chen, Z. H. Sun, J. H. Luo, M. C. Hong, *Cryst. Growth Des.*, 2012, **12**, 4109.

23. L. J. Dong, C. C. Zhao, X. Xu, Z. Y. Du, Y. R. Xie, J. Zhang, *Cryst. Growth Des.*, 2012, **12**, 2052.

24. L. F. Ma, L. Y. Wang, D. H. Lu, S. R. Batten, J. G. Wang, *Cryst. Growth Des.*,

2009, **9**, 1741.

25. H. Y. Liu, H. Wu, J. Yang, Y. Y. Liu, B. Liu, Y. Y. Liu, J. F. Ma, *Cryst. Growth Des.*, 2011, **11**, 2920.

26. Y. P. He, Y. X. Tan, J. Zhang, *Chem. Commun.*, 2013, **49**, 11323.

27. D. B. Shi, Y. W. Ren, H. F. Jiang, B. W. Cai, J. X. Lu, *Inorg. Chem.*, 2012, **51**, 6498.

28. H. J. Park, D. W. Lim, W. S. Yang, T. R. Oh, M. P. Suh, *Chem.− Eur. J.*, 2011, **17**, 7251.

29. A. Hagfeldt, G. Boschloo, L. C. Sun, L. Kloo, H. Pettersson, *Chem. Rev.*, 2010, **110**, 6595.

30. B. B. Hu, X. P. Chen, Y. F. Wang, P. Lu, Y. G. Wang, *Chem. – Asian. J.*, 2013, **8**, 1144.

31. H. R. Fu, Z. X. Xu, J. Zhang, *Chem. Mater.*, 2015, **27**, 205.

32. S. Yuan, Y. K. Deng, D. Sun, *Chem. – Eur. J.*, 2014, **20**, 10093.

33. H. R. Fu, Y. Kang, J. Zhang, *Inorg. Chem.*, 2014, **53**, 4209.

34. S. S. Liu, S. Yuan, X. Y. Li, S. Miao, Z. W. Yu, X. P. Wang, D. Sun, *Inorg. Chim. Acta.*, 2014, **416**, 195.

35. H. Wu, J. Yang, Z. M. Su, S. R. Batten, J. F. Ma, *J. Am. Chem. Soc.*, 2011, **133**, 11406.

36. H. Wu, H. Y. Liu. Y. Y. Liu, J. Yang, B. Liu, J. F. Ma, *Chem. Commun.*, 2011, **47**, 1818.

37. X. Q. Yao, Z. R. Pan, J. S. Hu, Y. Z. Li, Z. J. Guo, H. G. Zheng, *Chem. Commun.*, 2011, **47**, 10049.

38. M. D. Zhang, L. Qin, H. T. Yang, Y. Z. Li, Z. J. Guo, H. G. Zheng, *Cryst. Growth Des.*, 2013, **13**, 1961.

39. M. D. Zhang, C. M. Di, L. Qin, Q. X. Yang, Y. Z. Li, Z. J. Guo, H. G. Zheng, *CrystEngComm.*, 2013, **15**, 227.

40. C. Hua, P. Turner, D. M. D'Alessandro, *Dalton Trans.*, 2013, **42**, 6310.

41. L. J. Liu, K. Konstas, M. R. Hill, S. G. Telfer, *J. Am. Chem. Soc.,* 2013, **135,** 17731.

42. K. Sanjit, S. M. Partha, G. B. D. Michael, R. Joan, R. C. Nirmalendu, *Inorg. Chem.*, 2003, **42**, 2545.

43. Platon Program: A. L. Spek, *Acta Cryst. Sect. A.*, 1990, **46**, 194.

44. V. A. Blatov, A. P. Shevchenko, D. M. Proserpio, *Cryst. Growth Des.*, 2014, **14**, 3576.

45. S. S. Chen, R. Qiao, L. Q. Sheng, Y. Zhao, S. Yang, M. M. Chen, Z. D. Liu, D. H. Wang, *CrystEngComm.*, 2013, **15**, 5713.

46. L. Qin, J. S. Hu, M. D. Zhang, Y. Z. Li, H. G. Zheng, *CrystEngComm.*, 2012, **14**, 8274.

47. Y. Yang, P. Du, J. Yang, W. Q. Kan, J. F. Ma, *CrystEngComm.*, 2013, **15**, 4357.

48. S. Q. Zang, M. M. Dong, Y. J. Fan, H. W. Hou, T. C. W. Mak, *Cryst. Growth Des.*, 2012, **12**, 1239.

49. M. Tonigold, Y. Lu, A. Mavrandonakis, A. Puls, R. Staudt, J. Möllmer, J. Sauer, D. Volkmer, *Chem. – Eur. J.,* 2011, **17,** 8671.

50. J. Zhou, W. H. Fang, C. Rong, G. Y. Yang, *Chem. – Eur. J.*, 2010, **16**, 4852.

51. D. Sarma, K. V. Ramanujachary, S. E. Lofland, T. Magdaleno, S. Natarajan, *Inorg. Chem.*, 2009, **48**, 11660.

**Table 1.** Crystal data and structural refinements parameters of complexes **1-6**

Complexes	**1**[a]	**2**	**3**[a]	**4**[a]	**5**[a]	**6**[a]
Empirical formula	$C_{66}H_{72}N_{20}O_{27}Co_3$	$C_{32}H_{22}N_{10}O_4Co$	$C_{31}H_{28}N_{11}O_8Co$	$C_{104}H_{90}N_{32}O_{17}Co_2$	$C_{32}H_{29}N_{11}O_7Co$	$C_{33}H_{30}N_{10}O_7Co$
Formula weight	1754.20	669.52	741.56	2177.90	738.58	737.59
Temperature (K)	293(2)	293(2)	293(2)	123(2)	296(2)	296(2)
Crystal system	triclinic	orthorhombic	monoclinic	triclinic	triclinic	triclinic
Space group	$P\bar{1}$	$Pbca$	$C2/c$	$P1$	$P\bar{1}$	$P\bar{1}$
a / Å	10.0510(8)	10. 9941(10)	28.6457(12)	11.8012(10)	10.0885(10)	10.1017(4)
b / Å	17.7700(13)	20.2900(19)	12.5440(5)	15.9766(13)	11.3212(11)	11.4199(5)
c / Å	17.9534(13)	25.862(2)	21.6016(9)	16.0411(13)	15.8398(15)	15.8007(7)
α / °	67.2500(10)	90	90	111.8810(10)	97.102(2)	96.827(2)
β / °	74.9280(10)	90	103.1950(10)	107.7390(10)	93.075(2)	93.185(2)
γ / °	81.5690(10)	90	90	94.2350(10)	104.8080(10)	105.541(2)
V / Å^3	2851.6(4)	5769.0(9)	7557.2(5)	2612.3(4)	1728.8(3)	1736.39(13)
Z	1	8	8	1	2	2
D_{calcd} / g·cm^{-3}	0.927	1.542	1.272	1.350	1.384	1.376
μ / mm^{-1}	0.484	0.654	0.511	0.396	0.556	0.553
$F(000)$	815	2744	2976	1098	742	742
θ min-max / °	1.41, 25.00	1.57, 26.37	1.46, 25.00	1.47, 26.37	1.88, 25.00	1.87, 25.00
Tot., uniq. data	21376, 9930	45007, 5889	20818, 6658	21683, 15854	9436, 5989	9912, 6059
R(int)	0.0372	0.1372	0.0217	0.0283	0.0981	0.0593
Observed data [$I > 2\sigma(I)$]	7381	4132	5571	14189	5362	4494
N_{ref}, N_{par}	9930, 484	5889, 424	6658, 463	15854, 1368	5989, 446	6059, 450
GOF on F^2	1.028	1.018	1.059	1.067	1.069	1.074
R_1, wR_2 [$I > 2\sigma(I)$][b]	0.0513, 0.1623	0.0565, 0.1370	0.0553, 0.1761	0.0589, 0.1681	0.0668, 0.1863	0.0666, 0.1929
R_1, wR_2 (all data)	0.0657, 0.1727	0.0878, 0.1557	0.0625, 0.1832	0.0649, 0.1758	0.0716, 0.1925	0.0765, 0.2025
Min. and max resd dens (e ·Å^{-3})	-0.439, 0.445	-0.942, 0.518	-0.610, 0.840	-0.930, 0.892	-0.848, 0.953	-0.981, 0.964

[a] The residual electron densities were flattened by using the SQUEEZE option of PLATON.

[b] $R_1=\Sigma||F_o|-|F_c||/\Sigma|F_o|$, $wR_2=\{\Sigma[w(F_o^2-F_c^2)^2]/\Sigma[w(F_o^2)^2]\}^{1/2}$; where $w=1/[\sigma^2(F_o^2)+(aP)^2+bP]$, $P=(F_o^2+2F_c^2)/3$.

Syntheses, structures, and properties of six cobalt(II) complexes based on a tripodal tris(4-(1*H*-1,2,4-triazol-1-yl)phenyl)amine ligand

Zhenzhen Shi, Zhaorui Pan, Chuanlei Zhang, Hegen Zheng[*]
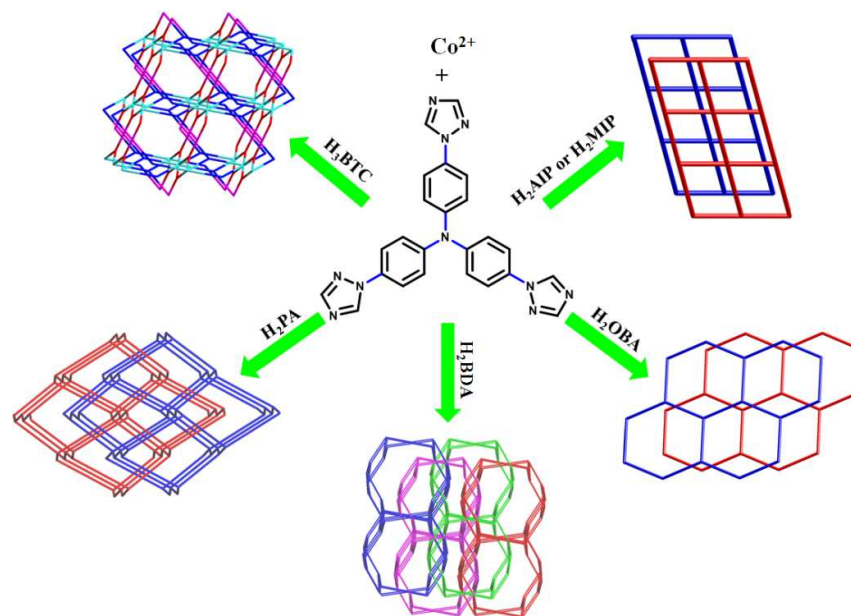
Six new cobalt(II) metal-organic frameworks based on the tripodal tris(4-(1H-1,2,4-triazol-1-yl)phenyl)amine (TTPA) ligand with different aromatic carboxylate auxiliary ligands have been synthesized and structurally characterized in detail. All the complexes show optical semiconductive properties.